COORDINATED PRODUCTION
FOR BETTER RESOURCE EFFICIENCY

D1.4 REPORT ON MODEL REDUCTION FOR OPTIMIZATION AND CONTROL

Carlos Vilas
Researcher at IIM-CSIC - Spain

March 2018
www.spire2030.eu/copro

This project has received funding from the European Union's Horizon 2020 research and innovation programme under grant agreement No 723575

Project Details

PROJECT TITLE	Improved energy and resource efficiency by better coordination of production in the process industries
PROJECT ACRONYM	**COPRO**
GRANT AGREEMENT NO	**723575**
INSTRUMENT	**RESEARCH AND INNOVATION ACTION**
CALL	**H2020-SPIRE-02-2016**
STARTING DATE OF PROJECT	**NOVEMBER, 1ST 2016**
PROJECT DURATION	**42 MONTHS**
PROJECT COORDINATOR (ORGANIZATION)	**PROF. SEBASTIAN ENGELL (TUDO)**

THE COPRO PROJECT

The goal of CoPro is to develop and to demonstrate methods and tools for process monitoring and optimal dynamic planning, scheduling and control of plants, industrial sites and clusters under dynamic market conditions. CoPro pays special attention to the role of operators and managers in plant-wide control solutions and to the deployment of advanced solutions in industrial sites with a heterogeneous IT environment. As the effort required for the development and maintenance of accurate plant models is the bottleneck for the development and long-term operation of advanced control and scheduling solutions, CoPro will develop methods for efficient modelling and for model quality monitoring and model adaption.

The CoPro Consortium

Participant No	Participant organisation name	Country	Organisation
1 (Coordinator)	Technische Universität Dortmund (TUDO)	DE	HES
2	INEOS Köln GmbH (INEOS)	DE	IND
3	Covestro Deutschland AG (COV)	DE	IND
4	Procter & Gamble Services Company NV (P&G)	BE	IND
5	Lenzing Aktiengesellschaft (LENZING)	AU	IND
6	Frinsa del Noroeste S.A. (Frinsa)	ES	IND
7	Universidad de Valladolid (UVA)	ES	HES
8	École Polytechnique Féderale de Lausanne (EPFL)	CH	HES
9	Ethniko Kentro Erevnas Kai Technologikis Anaptyxis (CERTH)	GR	RES
10	IIM-CSIC (CSIC)	ES	RES
11	LeiKon GmbH (LEIKON)	DE	SME
12	Process Systems Enterprise LTD (PSE)	UK	SME
13	Divis Intelligent Solutions GmbH (divis)	DE	SME
14	Argent & Waugh Ltd. (Sabisu)	UK	SME
15	ASM Soft S.L (ASM)	ES	SME
16	ORSOFT GmbH (ORS)	DE	SME
17	Inno TSD (inno)	FR	SME

Document details

DELIVERABLE TYPE	**REPORT**	
DELIVERABLE NO	**1.4**	
DELIVERABLE TITLE	**REPORT ON MODEL REDUCTION FOR OPTIMIZATION AND CONTROL**	
NAME OF LEAD PARTNER FOR THIS DELIVERABLE	**ANTONIO ÁLVAREZ ALONSO (CSIC)**	
VERSION	**1.1**	
CONTRACTUAL DELIVERY DATE	**30 APRIL 2018**	
ACTUAL DELIVERY DATE	**30 APRIL 2018**	
Dissemination level		
PU	Public	**X**
CO	Confidential, only for members of the consortium (including the Commission)	

Abstract

This report provides a description of the most efficient techniques for model reduction of systems of partial differential equations: the Laplacian spectral decomposition (LSD) and the Proper orthogonal decomposition (POD).

Model reduction techniques are compared in terms of simulation errors and reduction efficiency for a real scenario provided by FRINSA: the sterilization of packaged food. The POD technique is more efficient than the LSD for the same degree of accuracy. Also, the use of the POD technique is not limited to simulation but it can be used for a wider range of applications such as parameter estimation. The POD technique is therefore selected as the model reduction approach for PDE systems in the CoPro case studies.

REVISION HISTORY

The following table describes the main changes done in the document since it was created.

Revision	Date	Description	Author (Organisation)
V0.1	2 March 2018	Creation	C. Vilas (CSIC)
V0.2	23 March 2018	Description of reduction order techniques for PDEs	C. Vilas (CSIC)
V1.0	3 April 2018	Revision and quality control	J. L. Pitarch (UVA)
V1.1	5 April 2018	Implementation of reviewer suggestions	C. Vilas (CSIC)
V1.1	29 April 2018	Final approval	S. Engell (TUDO)

Disclaimer

Table of contents

1 Executive summary

The objective of Task 1.3 is to derive operational models suitable for real-time control and optimization by reducing the dimensionality, and therefore the computational load, of the systems of equations. The resulting models should be efficient as well as accurate.

During the first 16 months of the project different alternatives for model reduction in systems involving partial differential equations (PDEs) have been studied. In particular focus was on the Proper Orthogonal Decomposition (POD) and Laplacian Spectral Decomposition (LSD) because of their efficiency in dealing with PDE systems. Comparison of techniques during the first part of the project was based on the sterilization case study of the FRINSA partner. In particular, comparison was performed using RO-80 and RO-200 cans with tuna fish. The conclusion of this comparison is that the POD technique is more efficient than the LSD for the same degree of accuracy. Also, the use of the POD technique is not limited to simulation but it can be used for a wider range of applications such as parameter estimation. In the following months reduced order model for other can formats will be developed using the POD technique.

Also, these techniques will be applied to another case study in the FRINSA plant: thawing of fish.

2 Reduced order model for distributed process systems

Classical numerical methods for solving sets of PDEs, such as the finite differences method or the finite element method (FEM), usually result into a large number of ordinary differential equations to be solved. This drawback makes these approaches unsuitable for real-time tasks such as control or optimization. This is particularly relevant when considering 2D or 3D spatial domains.

Reduced order techniques have emerged as efficient alternatives to classical numerical methods. The main idea behind Reduced Order Models (ROMs) for PDE systems is to neglect the dynamics that occur at time scales much faster than the relevant ones.

ROMs have been applied to the simulation of a wide range of systems during the last six decades. Some examples include atmospheric modelling (Lorenz, 1960), turbulence simulation (Berkooz, et al., 1993), chemical reactors (Alonso, et al., 2004) or food engineering (Balsa-Canto, et al., 2002) among others. The advantages of using ROMs are not only limited to simulation but they have been successfully applied to efficiently handle problems in control (Shvartsman & Kevrekidis, 1998); parameter estimation (Vilas, et al., 2017); or observer design (García, et al., 2007) among others.

In the following section two of the most efficient methods for order reduction in PDEs will be described and illustrated through the sterilization of packaged food case study (FRINSA).

2.1 Theoretical aspects of reduced order models

Consider a given field $z(\xi, t)$ which may represent any state variable (for instance temperature; concentration of a given compound; pressure; etc). Consider also that the time evolution and spatial distribution of this variable is described by the following general PDE:

$$a\frac{\partial z}{\partial t} + \nabla \cdot (vz) = \kappa \Delta z + f(z) \tag{1}$$

defined on the (possibly 3D) spatial domain V with boundary B. For the sake of clarity, z is considered as a scalar field, although the same methodology applies to vector fields. a and κ are given parameters, v is the fluid velocity (zero for solids) and f is a, possibly nonlinear, scalar functions of the field. Symbols ∇, Δ represent the gradient and Laplacian operators.

In order to solve Eqn. (1) appropriate boundary and initial conditions are required. We will consider that boundary conditions (BC) take the following general form (Robin boundary conditions):

$$|n \cdot \kappa \nabla z + hz = g|_B \tag{2}$$

Note that Dirichlet boundary conditions, which indicate the value of the field in the boundary, can be approximated using Eqn (2) by selecting a large transfer coefficient h and $g = hz^{sm}$ where z^{sm} is the value of z on the surrounding media.

The *Fourier series theorem* (Reddy, 1998) plays a central role in the numerical techniques for solving PDEs. For this reason, a version of this theorem, suitable for the computations, will be first discussed. Essentially, the Fourier series theorem establishes that: given an orthonormal basis set on a Hilbert space ($\Phi = \{\phi_i(\xi)\}_{i=1}^{\infty}$) any function $s(\xi, t)$ can be expanded in convergent series of the form:

$$s(\xi, t) = \sum_{i=1}^{\infty} \langle \phi_i(\xi), s(\xi, t) \rangle_V \phi_i(\xi) = \sum_{i=1}^{\infty} r_i \phi_i(\xi)$$

The methods described in this section belong to the family of *methods of weighted residuals* (MWR) in which, the solution of the PDE (1) is approximated by truncating the series as follows:

$$z(\xi, t) \cong \tilde{z}(\xi, t) = \sum_{i=1}^{n} m_i(t) \phi_i(\xi) \tag{3}$$

The larger the number n, the better the approximation, so that in the limit when $n \to \infty$ it follows that $z = \tilde{z}$.

Instead of searching for the original solution $\big(z(\xi, t)\big)$, focus will be on computing the set of spatial dependent functions $\{\phi_i(\xi)\}_{i=1}^{n}$ (basis functions) and the time dependent functions $\{m_i(t)\}_{i=1}^{n}$ (modes).

The substitution of approximation (3) into Eqn (1) results into the following residual:

$$a\frac{\partial \tilde{z}}{\partial t} + \nabla \cdot (v\tilde{z}) - \kappa \Delta \tilde{z} - f(\tilde{z}) = R(\xi, t)$$

The best approximation will be that minimizing R and it is found by searching the set of modes which provides:

$$\int_V R(\xi, t) d\xi = 0$$

Multiplying this equation by n weighting functions $\psi(\xi)$ we obtain:

$$\int_V R(\xi, t) \psi_i d\xi = 0\,; \quad \text{with } i = 1,2, \dots, n$$

This system can be solved using any of the initial value problem solvers available. Depending on the selection of the weighting functions different methods arise. In this document we will focus on the *Galerkin* scheme (Reddy, 1993; Fletcher, 1984) where the weighting functions ψ_i coincide with the basis functions ϕ_i.

In this regard, the well known FEM uses locally defined basis functions. However, because their efficiency, we will focus on globally defined basis functions. In particular we will describe two of the most efficient techniques (Vilas, 2008): the Laplacian spectral decomposition (LSD) and the proper orthogonal decomposition (POD).

One important property of basis functions is that they are orthonormal, i.e.:

$$\int_V \phi_i \phi_j \mathrm{d}V = \begin{cases} 1 & \text{if } i = j \\ 0 & \text{if } i \neq j \end{cases} \tag{4}$$

In the following two sections the computation of the basis functions for the LSD and POD methods will be described. Besides, once the basis functions are known the procedure to compute the modes will be presented.

2.1.1 The Laplacian Spectral Decomposition

In this section the general aspects of this LSD are presented. For a detailed description see, for instance, (Rudin, 1991; Eidelman, et al., 2004). In this approach the basis functions are computed as the eigenfunctions of the Laplacian operator:

$$\kappa \Delta \phi_i(\xi) = -\lambda_i \phi_i(\xi) \tag{5}$$

This is a PDE system that requires appropriate boundary conditions to find a unique solution. Also in this approach such conditions must be homogeneous which is usually not the case in practice. Fortunately, a system with non homogeneous BC can be converted into an equivalent one with homogeneous BC by means of state transformations. This will be briefly presented in section 2.2.1, for details see (Emirsjlow & Townley, 2000). In this section, the methodology will be presented by considering the following homogeneous BC:

$$n \cdot \kappa \nabla \phi_i + h \phi_i = 0 \tag{6}$$

As shown in (Vilas, 2008) the matrices derived from the FEM can be used to numerically compute spatial integrals and derivatives. Table 1 summarizes the main relationships between the continuous operators and their discrete FEM counterparts. Matrices $\mathcal{M}, \mathcal{C}, \mathcal{D}$ and $\mathcal{B}$ are the mass, convective, diffusive and boundary matrices derived from the FEM. These matrices can be obtained for the 1D case using the Matmol toolbox (freely available at www.matmol.org). For 2D and 3D the commercial software COMSOL® can be used.

Table 1. Equivalence between the matrices derived from the FEM and continuous operators (spatial integral and derivatives). $f(\xi), g(\xi)$ are given functions with F, G being their discrete FEM counterparts.

Continuous operator	FEM equivalent
$\int_V f(\xi) g(\xi) \mathrm{d}V$	$F^T \mathcal{M} G$
∇	$\mathcal{M}^{-1} \mathcal{C}$
Δ	$\mathcal{M}^{-1} (\mathcal{D} + \mathcal{B})$

In this regard, PDE (5) with BC (6) is transformed into the following discrete eigenvalue problem:

$$\mathcal{M}^{-1}(\kappa\mathcal{D} + h\mathcal{B})\phi_i = -\lambda_i\phi_i$$

Once the basis functions are available we have to compute the modes. To that purpose, Eqn (1) is projected onto the basis functions. Mathematically this is carried out by multiplying Eqn (1) by each basis function and integrating the result over the spatial domain, i.e.:

$$a\int_V \phi_j \frac{\partial z}{\partial t}\mathrm{d}V + \int_V \phi_j \nabla\cdot(vz)\mathrm{d}V = \kappa\int_V \phi_j \Delta z \mathrm{d}V + \int_V \phi_j f \mathrm{d}V$$

Substituting the state variable $z(\xi,t)$ by its Fourier series expansion:

$$a\int_V \phi_j \frac{\partial \sum_{i=1}^{n}\phi_i m_i}{\partial t}\mathrm{d}V + \int_V \phi_j \nabla\cdot\left(v\sum_{i=1}^{n}\phi_i m_i\right)\mathrm{d}V = \kappa\int_V \phi_j \Delta\sum_{i=1}^{n}\phi_i m_i\,\mathrm{d}V + \int_V \phi_j f\mathrm{d}V$$

Taking into account that the basis functions only depend on the spatial coordinates and the modes only depend on time, we can sort previous equation as:

$$\begin{aligned} a\sum_{i=1}^{n}\frac{\mathrm{d}m_i}{\mathrm{d}t}\int_V \phi_j\phi_i\,\mathrm{d}V + \sum_{i=1}^{n} m_i\int_V \phi_j\nabla\cdot(v\phi_i)\mathrm{d}V \\ = \kappa\sum_{i=1}^{n} m_i\int_V \phi_j\Delta\phi_i dV + \int_V \phi_j f\mathrm{d}V \end{aligned} \tag{7}$$

Using the orthogonality property of the eigenfunctions -see Eqn (4)- and the eigenvalue problem – Eqn (5)-, previous equation can be simplified as:

$$a\frac{dm_j}{dt} + A_j m = -\lambda_j m_j + \int_V \phi_j f\mathrm{d}V \tag{8}$$

With $m = [m_1, m_2, \dots, m_n]^T$ and A_j is the *j*th row of matrix A whose elements are of the form:

$$A_{i,j} = \int_V \phi_j\nabla\cdot(v\phi_i)\mathrm{d}V$$

Extending Eqn. (8) to all $j = 1,2,\dots,p$ the following system of ODEs is obtained:

$$a\frac{dm}{dt} + Am = -\Lambda m + F; \qquad F_j = \int_V \phi_j f\mathrm{d}V; \qquad \Lambda_{ij} = \begin{cases}\lambda_j & if \quad i=j\\ 0 & otherwise\end{cases}$$

Again, the FEM matrices (Table 1) can be used to compute matrix A and vector F. This system can be solved using an appropriate IVP solver. Since the basis functions and the modes are available, the original state $z(\xi,t)$ can be recovered. In section 2.2.1 this technique will be applied to the sterilization of packaged food (FRINSA case study).

2.1.2 The Proper Orthogonal Decomposition

This technique, first proposed by Sirovich (1987), has been employed in many different fields like chemical reactors (Alonso, et al., 2004), biological systems (Vilas, et al., 2008), fluid dynamics (Berkooz, et al., 1993), among many others.

In this report, we will only consider the discrete formulation of the problem since, in practice, only a finite discrete set of measurements is available.

Let $\mathcal{Z}_i \in \mathbb{R}^n$ be the vector of values of the state $z(\xi, t)$ at a finite number (n) of spatial points and at a given time t_i. Such vector will be referred to as *snapshot*. The problem is stated as follows: Given a set of snapshots $\Im = \{\mathcal{Z}_i\}_{i=1}^k$, find a basis $\Phi = [\phi_1, \phi_2, \dots, \phi_p]$ which maximizes the projection over the original set $\Im$. Mathematically, this is formulated as (Holmes, et al., 1997):

$$\max_{\phi} J, \qquad with \;\; J = \frac{1}{k}\sum_{i=1}^{k}\left(\int_V \phi\, \mathcal{Z}_i\right)^2 - \lambda\left(\left(\int_V \phi\,\phi\right) - 1\right)$$

with k being a sufficiently large number of snapshots representative of the system and its dynamic behavior. The solution of this optimization problem leads to the following eigenvalue problem (Holmes, et al., 1997):

$$\int_V \mathcal{K}(\xi, \xi')\phi_i(\xi')d\xi' = \lambda_i \phi_i(\xi) \tag{9}$$

where the kernel ($\mathcal{K}$), in its discrete version, corresponds to a two point correlation kernel of the form:

$$\mathcal{K} = \frac{1}{k}\sum_{i=1}^{k} \mathcal{Z}_i \mathcal{Z}_i' \tag{10}$$

The FEM matrices (Table 1) can also help in the computation of the POD basis. In this regard, the integral eigenvalue problem (9) can be numerically solved as:

$$\lambda_i \phi_i = \mathcal{K}\mathcal{M}\phi_i \tag{11}$$

State measurements ($\mathcal{Z}_i$) can be obtained either from numerical simulation or from experiments. The term POD will be employed to denote the eigenfunctions obtained with this technique. The set of PODs forms a complete orthonormal basis set on a Hilbert space. Since $\mathcal{K}$ is real symmetric, its eigenvalues are real numbers (Courant & Hilbert, 1989). Note that the POD method provides a set of empirical basis functions which are optimal with respect to other possible expansions. This set is optimal in the sense that for a given number of basis functions, it captures most of the relevant dynamic behavior of the original distributed system in the range of initial conditions, parameters, inputs, and/or perturbations of the experimental data (Balsa-Canto, et al., 2004).

It must be pointed out that, for large values of n, solving Eqn (9) can be computationally involved. In order to avoid this problem and save computation time, a useful alternative, proposed by Sirovich (1987) and known as the *method of snapshots*, is briefly discussed. In this method, each eigenfunction is expressed in terms of the original data as:

$$\phi_j = \sum_{i=1}^{k} w_i^j \mathcal{Z}_i \tag{12}$$

with w_i^j being the weights to be computed.

Introducing Eqns (10) and (12) in the eigenvalue problem (9), results into:

$$\mathcal{Q}\mathcal{W}_j = \lambda_j \mathcal{W}_j$$

where the eigenvectors $\mathcal{W}_j$ have as elements the weights in equation (12) so that $\mathcal{W}_j = [w_1^j, w_2^j, \dots, w_k^j]$. The elements of matrix $\mathcal{Q}$ are defined as:

$$Q_{i,j} = \frac{1}{k}\int_V Z_i Z_j \mathrm{d}V$$

Both the direct method and the method of snapshots are implemented in the Matlab® function *matpod* of the Matmol toolbox.

Eigenvalues (λ_i) can be employed as an *a priori* measurement of the approximation accuracy. In this sense, the total energy captured by the full set of PODs is computed through the eigenvalues as $E = \sum_{i=1}^{n} \lambda_i$. Therefore the percentage of energy captured by a given number p of PODs is:

$$E(\%) = 100\frac{\sum_{i=1}^{p} \lambda_i}{\sum_{i=1}^{n} \lambda_i}$$

The more the energy captured, the better the quality of the approximation.

Note that, since the kernel is computed from a set of experimental measurements, the validity POD method will highly depend on the selection of such set. If it is poorly chosen the method will not properly work (Vilas, 2008). The experimental data must be chosen so it is representative of the dynamic behavior of the system.

Now that the computation of the basis functions was described, let us explain how to compute the modes. The procedure is the same as in the LSD case, i.e. by multiplying Eqn (1) by each basis function and integrating the result over the spatial domain. The main difference is that in this case the basis functions do not fulfill the eigenvalue problem (5) so, if we consider Eqn (7), taking into account the POD basis orthonormality property we obtain, for each POD basis:

$$a\frac{dm_j}{dt} + A_j m = \kappa \mathcal{P}_j m + \int_V \phi_j f \mathrm{d}V$$

With $m = [m_1, m_2, \dots, m_n]^T$. A_j and $\mathcal{P}_j$ are the *j*th rows of matrices A and $\mathcal{P}$ whose elements are of the form:

$$A_{i,j} = \int_V \phi_j \nabla \cdot (v\phi_i)\mathrm{d}V\,; \qquad \mathcal{P}_{i,j} = \int_V \phi_j \Delta\phi_i \mathrm{d}V$$

Projection over all the basis functions leads to the following system of ODEs:

$$a\frac{dm}{dt} + Am = \kappa \mathcal{P} m + F; \qquad F_j = \int_V \phi_j f \mathrm{d}V$$

2.2 Application to the FRINSA case study: temperature distribution inside the packaged food during sterilization

In this case sterilization is performed by applying high temperatures (in the range of 110-125 ℃) to the packaged food during a given period of time. At the beginning of the process all the product is at ambient temperature (5-30 ℃). As the process evolves product temperature increases, and the increase is faster at those points closer to the can boundaries. Lethality of microorganisms (F_0) is computed using the temperature at the coldest point of the food product (T_c), which is usually located at the center of the product, as:

$$\frac{dF_0}{dt} = 10^{\frac{T_c - T_{ref}}{z_{ref}}}$$

where T_{ref}, z_{ref} are given parameters whose value depend on the bacteria considered. At the same time, temperature affects food quality (color, nutrient retention, etc). Therefore, in order to compute the safety and quality parameters, temperature evolution and spatial distribution are required.

A picture of the real can is presented in Figure 1. If the can is homogeneously heated (as it is usually the case) then the 3D problem can be reduced to a 2D problem in cylindrical coordinates (z, r). Furthermore, symmetry allows us considering just half of the whole spatial domain (shaded region in the Figure) by selecting no flux boundary conditions (these BC have the form of Eqn (2) with $h = 0, g = 0$).

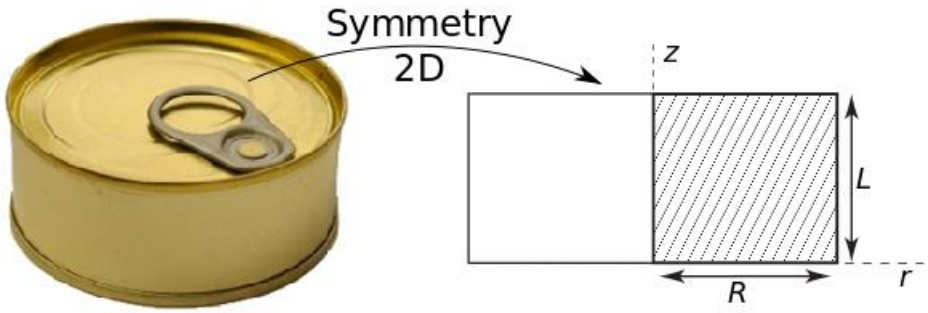

Figure 1. Picture of a real (3D) cylindrical can (left). Symmetry properties allow reducing the dimensionality to a 2D problem (right)

The heat equation is used to describe the evolution of the temperature inside the can:

$$\rho c_p \frac{\partial T}{\partial t} = \kappa \Delta T \tag{13}$$

where ρ, c_p and κ are, respectively, the density, specific heat and thermal conductivity of the packaged food (in this case tuna). Symbol Δ represents the Laplacian operator in cylindrical coordinates, i.e.

$$\Delta = \frac{\partial^2}{\partial z^2} + \frac{1}{r}\frac{\partial}{\partial r}\left(r\frac{\partial}{\partial r}\right)$$

with z, r being, respectively, the height and the radius of the product.

At the product top, a layer of filling fluid separates the metal cover from the product so heat flux boundary conditions are considered:

$$n \cdot \kappa \nabla \mathrm{T}|_{z=L} = h(T|_{z=L} - T_{sm}) \quad \forall r \tag{14}$$

T_{sm} denotes the temperature of the surrounding media (sterilization temperature). At the right and bottom boundaries the metal cover is in contact with the product so the transfer coefficient will be large and Dirichlet boundary conditions are considered:

$$\mathrm{T}|_{z=0} = \mathrm{T}|_{r=R} = T_{sm}$$

As mentioned above, these boundary conditions can be approximated by Robin boundary conditions of the form:

$$n \cdot \kappa \nabla \mathrm{T}|_{z=0} = h^*(T|_{z=0} - T_{sm}) \quad \forall r \tag{15}$$

$$n \cdot \kappa \nabla \mathrm{T}|_{r=R} = h^*(T|_{r=R} - T_{sm}) \quad \forall z \tag{16}$$

where $h^*$is a large value which will depend on the problem, in this case $h^* = 5000\ W/(m^2°\mathrm{C})$ is enough to approximate Dirichlet boundary conditions.

At the left boundary, symmetry boundary conditions are considered:

$$n \cdot \kappa \nabla \mathrm{T}|_{r=0} = 0 \quad \forall z \tag{17}$$

In the following two sections we will apply the LSD and the POD method to this problem.

2.2.1 Application of the Laplacian Spectral Decomposition

As mentioned above, this approach requires boundary conditions to be homogeneous. Since boundary conditions (14)-(16) are non-homogeneous, a new system with homogenous BC will be derived. To that purpose, a new state variable is defined as:

$$y(r,z,t) = T(r,z,t) - \chi(r,z)\pi(t) \tag{18}$$

Choosing $\chi(r,z) = 1;\ \pi(t) = T_{sm}$ and substituting Eqn (18) into system (13)-(17) we obtain:

$$\rho c_p \frac{\partial y}{\partial t} = \kappa \Delta y - \rho c_p \frac{\mathrm{d}T_{sm}}{\mathrm{d}t} \tag{19}$$

with homogeneous boundary conditions of the form:

$$n \cdot \kappa \nabla \mathrm{y}|_{z=L} = hy|_{z=L} \quad \forall r$$
$$n \cdot \kappa \nabla \mathrm{y}|_{z=0} = h^* y|_{z=0} \quad \forall r$$
$$n \cdot \kappa \nabla \mathrm{y}|_{r=R} = h^* y|_{r=R} \quad \forall z$$
$$n \cdot \kappa \nabla \mathrm{y}|_{r=0} = 0 \quad \forall z$$

Applying the Fourier series expansion to field $y(r,z,t)$ results into:

$$y(r,z,t) = \sum_{i=1}^{p} m_i(t)\phi_i(r,z) \tag{20}$$

Basis function are obtained by solving the eigenproblem problem:

$$\kappa \Delta \phi_i(r,z) = -\lambda_i \phi_i(r,z)$$

with boundary conditions:

$$|n \cdot \kappa \nabla \phi_i = h\phi_i|_{z=L}$$
$$|n \cdot \kappa \nabla \phi_i = h^*\phi_i|_{z=0}$$
$$|n \cdot \kappa \nabla \phi_i = h^*\phi_i|_{r=R}$$
$$|n \cdot \kappa \nabla \phi_i = 0|_{r=0}$$

Again, the FEM matrices can be employed to approximate the PDE eigenvalue problem by a discrete eigenvalue problem:

$$\mathcal{M}^{-1}\left(\kappa \mathcal{D} + h\mathcal{B}_{top} + h^*\mathcal{B}_{br}\right)\phi_i = -\lambda_i \phi_i$$

Where $\mathcal{M}, \mathcal{D}, \mathcal{B}_{top}$ and $\mathcal{B}_{br}$ are, respectively, the mass, diffusion and boundary matrices of the FEM.

A major disadvantage of this method is that, for every combination of parameters κ, h, h^*, a different set of basis functions must be obtained so it cannot be used for parameter estimation purposes. The way to proceed for a real case study should be first computing the value of the parameters using

other technique (for instance the FEM). Once the parameters are available, the LSD approach could be employed for simulation and optimization.

For the sake of illustration let us consider the following parameter values: $\kappa = 0.45, h = 50, h^* = 5000$. Figure 2 shows the spatial distribution of the first four basis functions.

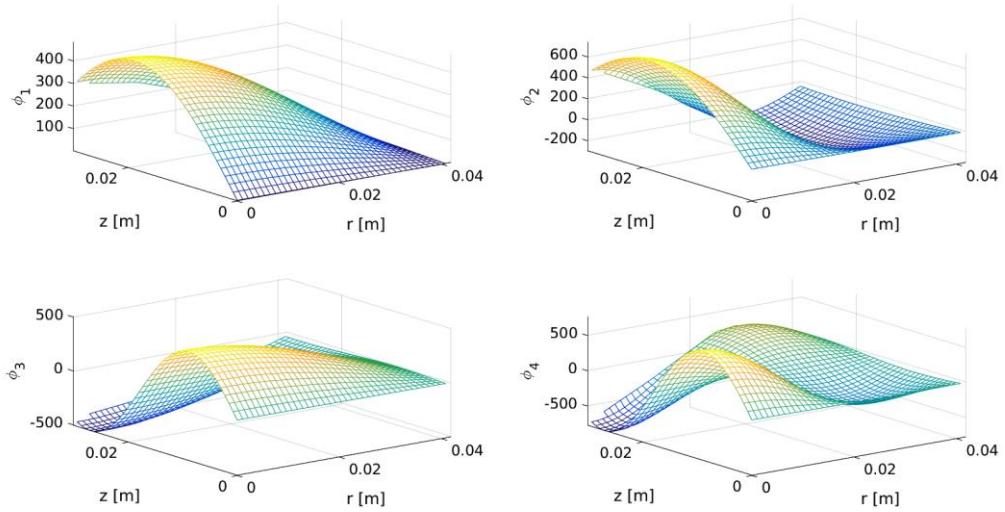

Figure 2. Spatial distribution of the first basis functions from the LSD method for the state variable $y(r, z, t)$

Once the basis functions are available we need to compute the modes. This is performed by following the procedure described in section 2.1.1. Let us summarize here the main steps. First we multiply Eqn (19) by a given basis function and integrate on the spatial domain:

$$\rho c_p \int_V \phi_j \frac{\partial y}{\partial t} dV = \kappa \int_V \phi_j \Delta y dV - \rho c_p \int_V \phi_j \frac{\mathrm{d}T_{sm}}{\mathrm{d}t} dV$$

Using the Fourier series approximation and sorting terms

$$\rho c_p \sum_{i=1}^{p} \frac{\mathrm{d}m_i}{\mathrm{d}t} \int_V \phi_j \phi_i dV = \sum_{i=1}^{p} m_i \int_V \phi_j \kappa \Delta \phi_i dV - \rho c_p \int_V \phi_j \frac{\mathrm{d}T_{sm}}{\mathrm{d}t} dV$$

Since eigenfunctions are orthogonal, using the eigenvalue problem and extending the result to $j = 1,2, \dots, p$ leads to the following set of ODEs:

$$\rho c_p \frac{\mathrm{d}m}{\mathrm{d}t} = -\Lambda m - \rho c_p F; \qquad F = \int_V \phi_j \frac{\mathrm{d}T_{sm}}{\mathrm{d}t} dV$$

This ODE system can be solved using an appropriate IVP solver.

Now we have the modes and the LSD basis so we can recover the original solution $y(r, z)$ by using Eqn (20) and therefore $T(r, z)$ using Eqn (18).

In order to illustrate the reduction capabilities of the LSD method a comparative example will be used. In this example the value of the ambient temperature (T_{sm}) is taken from a real experiment performed in FRINSA. Comparison is performed in terms of the absolute and relative errors with respect to the FEM:

$$Abs.Error = |T_{FEM} - T_{LSD}|; \qquad Rel.Error = \frac{|T_{FEM} - T_{LSD}|}{T_{FEM}} 100$$

Table 2 shows the comparison results. Different number of terms in the Fourier expansion has been considered. As shown in the Table, there is a large improvement in mean values between using $p = 20$ and $p = 50$. However, from $p > 50$ errors are not significantly reduced. This is because, since T_{sm} is taken from a real case with a given measurement error, we are not able to accurately compute $\mathrm{d}T_{sm}/\mathrm{d}t$ and therefore this small error is transmitted to the solution. For simulation purposes we can consider that models with $p \geq 50$ are adequate for representing the behavior of the system.

Table 2. Comparison, in terms of the absolute and relative errors, between the classical finite element method and the LSD approach with different number of elements for the FRINSA case study

		FEM	LSD			
	N. ODEs	1097	20	50	100	200
Absolute Error (℃)	Maximum	-	16.6	14.0	12.8	12.8
	Mean	-	0.26	0.14	0.13	0.13
Relative Error (%)	Maximum	-	53.8	38.7	34.8	31.8
	Mean	-	0.47	0.25	0.22	0.21

Figure 3 shows the solution with the FEM and the LSD. In this regard, top left figure shows the evolution at three different points inside the can obtained with the LDS (continuous lines) and the FEM (marks). Black line represents the measured retort temperature. Top right figure shows the evolution of the maximum (black line) and mean (blue line) absolute errors. As expected the larger errors are produced when the retort temperature rapidly changes, i.e. at the beginning of the process and at the beginning of the cooling stage, then these errors rapidly converge to values close to zero. Errors at the beginning of the process are not relevant for quality and safety issues since the temperature is low. Errors at the beginning of the cooling stage are not very large. Bottom figures represent the temperature distribution inside the food package at a given time (left) and the corresponding distribution of the absolute error. Note that, this error is never larger than 0.2 ℃ which is below the thermocouple measurement error. The LSD reduces in around one order of magnitude the number of equations of the FEM.

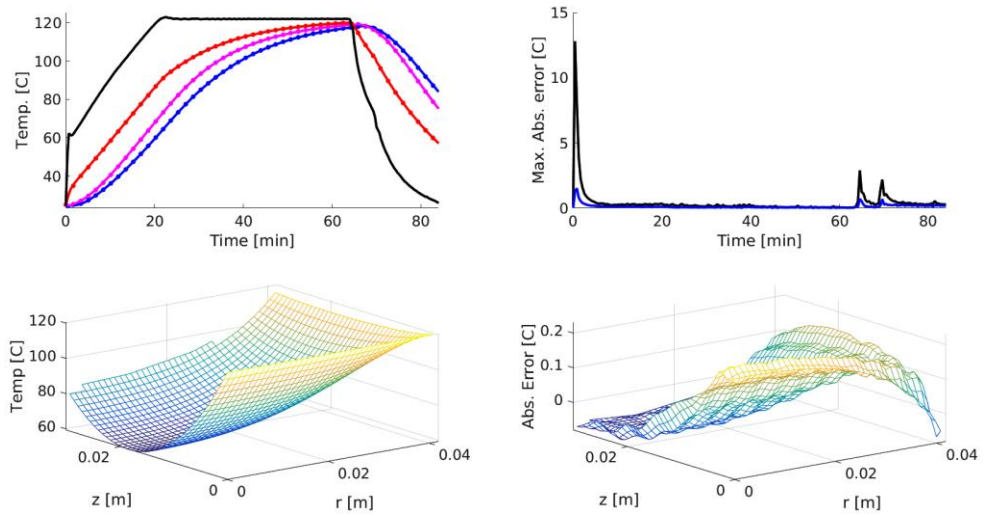

Figure 3. Comparison between the FEM and the LSD method with $p = 200$. Top left figure: Evolution of the temperature at three different spatial locations (blue, $r = 0, z = L/2$; magenta, $r = R/3, z = 3L/2$; red, $r = 2R/3, z = L$). Continuous lines represent the POD solution whereas dots correspond to the FEM. Black line is the retort temperature. Top right figure: Evolution of the maximum and mean absolute error. Bottom left figure: snapshot of the temperature obtained with the POD method at $t = 24$ min. Bottom right figure: spatial distribution of the absolute error at $t = 24$ min.

2.2.2 Application of the Proper Orthogonal Decomposition

As mentioned in section 2.1.2, the first step of the POD is to obtain a set of snapshots representative of the system behavior. Such snapshots can be obtained either taking measurements in the real process or performing numerical simulations. Due to the huge amount of sensors required to obtain good snapshots experimentally, the second approach (numerical simulation using the FEM) will be used. Besides, the FEM will be also used to compare the simulation results. However, in order to run the simulations, parameters ρ, c_p, κ, h must be known. Two options arise:

- Parameters are estimated from experimental data using, for instance, the FEM and then the snapshot are obtained using the computed values
- Simulations are performed for different combinations of parameters and all the snapshots obtained for each combination are used to compute the POD basis

In the first case, the resulting model will be more efficient than in the second case. However, the second case will allow us to use the model in a wider range of conditions what will enable its use for parameters estimation as well. The second approach is selected.

The main problem when model (13)-(17) is used for parameter estimation purposes is that, as shown in (Vilas, et al., 2017), it is not structurally identifiable. In other words, a unique value for all parameters cannot be found. However, an equivalent identifiable model can be obtained by dividing the system of equations by ρc_p:

$$\frac{\partial T}{\partial t} = \alpha \Delta T \tag{21}$$

$$n \cdot \alpha \nabla \mathrm{T}|_{z=L} = h_g(T|_{z=L} - T_{sm}) \quad \forall r$$

$$n \cdot \alpha \nabla \mathrm{T}|_{z=0} = h_g^*(T|_{z=0} - T_{sm}) \quad \forall r$$

$$n \cdot \alpha \nabla \mathrm{T}|_{r=R} = h_g^*(T|_{r=R} - T_{sm}) \quad \forall z$$

$$n \cdot \alpha \nabla \mathrm{T}|_{r=0} = 0 \quad \forall z$$

with

$$\alpha = \frac{\kappa}{\rho c_p}; \quad h_g = \frac{h}{\rho c_p}$$

Instead of four unknown parameters, now we have a model that produces the same simulation results with two (identifiable) unknown parameters (α, h_g).

Let us now start with the derivation of the ROM using the POD. The solution $T(r,z,t)$ is approximated using a truncated Fourier series of the form:

$$T(r,z,t) = \sum_{i=1}^{p} \phi_i(r,z) m_i(t) \tag{22}$$

The basis functions are computed by solving the eigenvalue problem

$$\lambda_i \phi_i = \mathcal{K}\mathcal{M}\phi_i \tag{23}$$

$$\mathcal{K} = \frac{1}{k}\sum_{i=1}^{k} \mathcal{T}_i \mathcal{T}_i' \tag{24}$$

with $\mathcal{T}_i \in \mathbb{R}^n$ being the snapshot of the temperature at time t_i. Snapshots are obtained from simulations using different combinations of parameters. Table 3 shows the values of the parameters considered in the simulations. Note that this implies performing 250 simulations. In each simulation 200 snapshots were taken so the total number of snapshots used to obtain the POD basis is 5×10^4. The values of α were selected according to the values reported in the bibliography whereas the values of h_g were selected in order to represent both heat flux conditions (low values) and Dirichlet boundary conditions (large values).

Table 3. Range of parameter values considered for FEM simulation

	α	h_g
Range	Ten points equally distributed in the range $[0.718 \times 10^{-7}, 3.589 \times 10^{-7}]$	Twenty-five points distributed in logarithmic scale in the range $[2.392 \times 10^{-8}, 1.196 \times 10^{-3}]$

Furthermore, there are two variables that may change from one experiment to another: the retort temperature and the initial conditions. In order to cover the whole range of retort temperatures, five steps (randomly selected between $105 - 130$ ℃) were considered for each experiment. This is shown in the left figures of Figure 4 (black line). The control profile (retort temperature) is not the same in the first experiment than in the second one. In the same way, each simulation started from initial conditions randomly chosen in the range 5-30 ℃.

Figure 4 also includes plots of the temperature distribution inside the food product at a given time (right figures). This is what we refer to as *snapshot*.

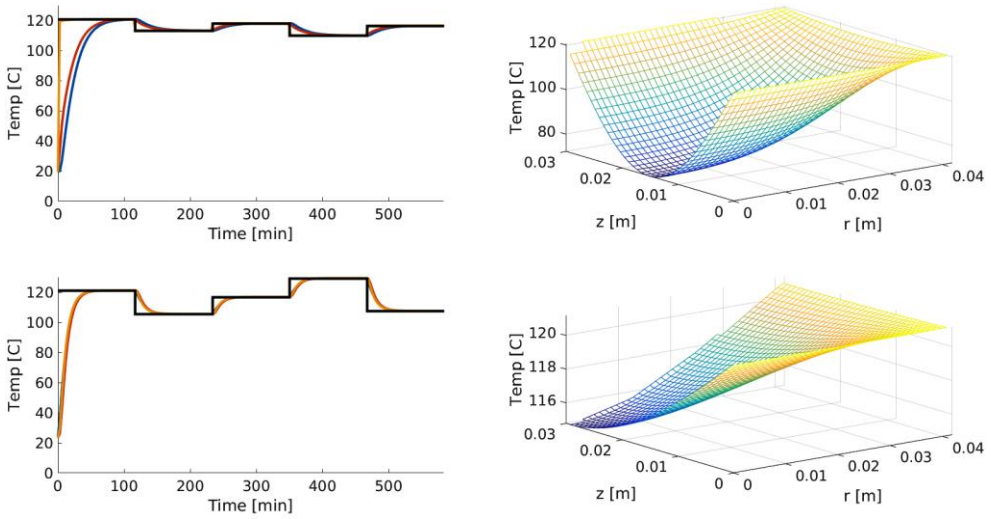

Figure 4. Simulation results for two experiments carried out to obtain the set of snapshots. Left figures : Time evolution of the retort temperature (black line) and three points inside the can (blue, red and orange lines). Right figures : spatial distribution of the temperature at a given time during the experiment. Values used for the parameters in the top experiment are : $\alpha = 0.718 \times 10^{-7}, h_g = 6.924 \times 10^{-4}$ whereas in the bottom experiments such parameters are : $\alpha = 2.951 \times 10^{-7}, h_g = 2.131 \times 10^{-8}$.

Now that we have the snapshots, kernel (24) is constructed and the POD basis are computed by solving Eqn (23). The first four POD basis are represented in Figure 5. The first POD is almost flat as it is usually the case. POD basis with lower spatial oscillations are more representative. As mentioned above, relevance of the POD basis can be also inferred from the associated eigenvalue: the larger the value of the eigenvalue the more relevant the POD basis is. In this case, $\lambda_1 = 3.55 \times 10^{-1}; \lambda_2 = 4.19 \times 10^{-4}$; $\lambda_3 = 3.51 \times 10^{-5}$; $\lambda_4 = 8.66 \times 10^{-6}$.

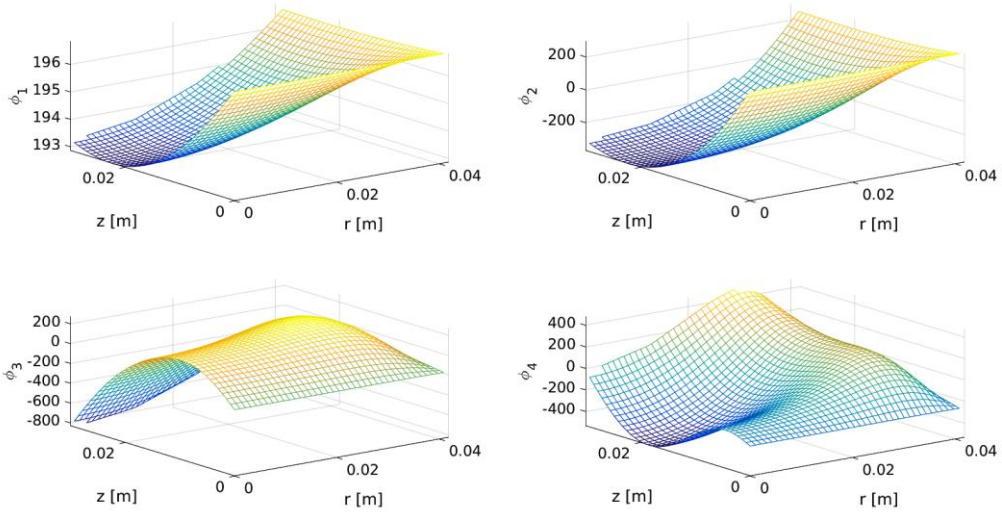

Figure 5. Spatial distribution of the first four POD basis.

These POD basis are valid for RO200 cans. For other type of cans new snapshots must be obtained from simulations and the same procedure applies.

The next step is to obtain the set of modes $\{m_i\}_{i=1}^{p}$ by following the procedure described in Section 2.1.2, i.e. Eqn (21) is projected over the set of POD basis. Let us consider the POD basis ϕ_j:

$$\int_V \phi_j \frac{\partial T}{\partial t} dV = \alpha \int_V \phi_j \Delta T dV$$

Using the Fourier series expansion to approximate the temperature and taking into account that the POD basis do not depend on time and the modes do not depend on the spatial coordinate we obtain:

$$\int_V \phi_j \sum_{i=1}^{p} \phi_i \frac{\mathrm{d}m_i}{\mathrm{d}t} dV = \alpha \int_V \phi_j \sum_{j=1}^{p} m_i \Delta \phi_i \, dV$$

Since the POD basis are orthonormal -see Eqn (4)- we have:

$$\frac{\mathrm{d}m_j}{\mathrm{d}t} = \alpha \sum_{j=1}^{p} m_j \int_V \phi_i \Delta \phi_j dV$$

Extending this equation to all $j = 1,2, \dots, p$ and defining the vector of modes as $m = [m_1, m_2, \dots, m_p]^T$ we obtain the following set of ODEs:

$$\frac{\mathrm{dm}}{\mathrm{d}t} = \alpha A m; \quad \text{with} \quad A_{i,j} = \int_V \phi_i \Delta \phi_j dV$$

Matrix A can be numerically computed using the FEM matrices (Table 1). This system of ODEs can be solved using an appropriate initial value problem (IVP) solver.

Now we have the modes and the POD basis so we can recover the original solution $T(r, z, t)$.

As in the LSD case, a real experiment carried out at the FRINSA plant is used to illustrate the reduction capabilities of the POD method. To that purpose different number of terms is considered in Fourier expansion and the results are compared against the solution obtained the FEM in terms of absolute and relative errors:

$$Abs.Error = |T_{FEM} - T_{POD}|; \quad Rel.Error = \frac{|T_{FEM} - T_{POD}|}{T_{FEM}} 100$$

Table 4 shows the results of such comparison. Parameter values in this simulation are different from those considered in the battery of simulations performed to obtain the snapshots ($\alpha = 1.29 \times 10^{-7}$ and $h_g = 5.81 \times 10^{-5}$).

Note that for models with $p \geq 9$, mean absolute error remains close to or below 0.1 ºC. A maximum absolute error of 5.8 and 4.1ºC is obtained with $p = 9, 12$ respectively. However these errors are just close to the beginning of the process where the temperature is very low and therefore they do not affect quality and safety parameters. Also, these errors rapidly converge to values below 0.1 ºC. Therefore, using $p \geq 9$ results into adequate models for representing the behavior of the system. The same conclusions can be drawn for other experimental conditions. Note that the number of equations to be solved is two orders of magnitude lower than in the FEM.

Table 4. Comparison, in terms of relative and absolute errors, between the FEM and the POD method with different number of elements (p)

		FEM	POD			
	N. ODEs	1097	3	6	9	12
Absolute	Maximum	-	18.0	12.5	5.8	4.1

Error (℃)	Mean	-	1.8	0.31	0.11	0.06
Relative Error (%)	Maximum	-	67.5	36.0	15.7	15.1
	Mean	-	2.6	0.49	0.18	0.10

The comparison between the solutions obtained with the FEM and the POD with $p = 12$ is presented in Figure 6. Top left figure shows the evolution at three different points inside the can obtained with the POD (continuous lines) and the FEM (marks). Black line represents the measured retort temperature. As shown in the Figure continuous lines and marks coincide. Top right figure shows the evolution of the maximum (black line) and mean (blue line) absolute errors. As mentioned above larger errors correspond with rapid changes in the retort temperature (beginning of the process). As in the LSD case, errors at the beginning of the cooling stage are not very large. Bottom figures represent the temperature distribution inside the food package at a given time (left) and the corresponding distribution of the absolute error. Note that, this error is never larger than 0.3 ℃, except for one point in the product boundary, and in any case simulation errors remain below the thermocouple measurement error.

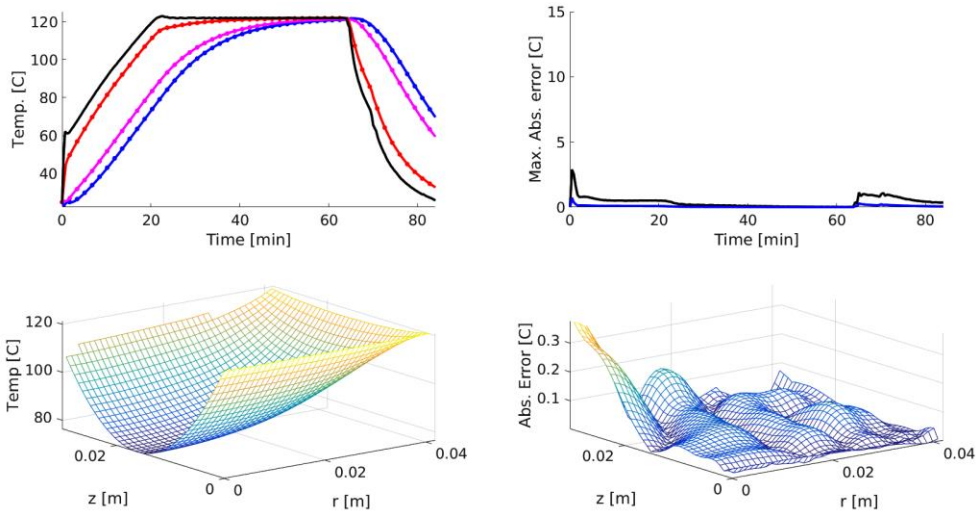

Figure 6. Comparison between the FEM and the POD with $p = 12$. Top left figure : Evolution of the temperature at three different spatial locations (blue, $r = 0, z = L/2$; magenta, $r = R/3, z = 3L/2$; red, $r = 2R/3, z = L$). Continuous lines represent the POD solution whereas dots correspond to the FEM. Black line is the retort temperature. Top right figure: Evolution of the maximum and mean absolute error. Bottom left figure: snapshot of the temperature obtained with the POD method at $t = 24$ min. Bottom right figure: spatial distribution of the absolute error at $t = 24$ min.

2.3 Conclusions

In this section two of the most efficient techniques for model reduction of PDE systems have been described: the Laplacian spectral decomposition and the Proper orthogonal decomposition. Model reduction in both cases has been illustrated for the sterilization of RO200 cans using a real experiment carried out at FRINSA plant. The same procedure can be applied for other distributed process systems such as, for instance, other type of cans or thawing of fish.

Both techniques are able to reduce the number of equations with a satisfactory degree of accuracy however the POD method is preferable for two reasons:

- The POD method is more efficient than the LSD. The resulting number of equations in the sterilization case study is almost one order of magnitude lower in the POD method for the same degree of accuracy
- The LSD requires the computation of a new set of basis functions for each combination of parameters. However in the POD technique the same set of basis functions can be used for all the combinations of parameters. This enables the use of the POD for parameter estimation purposes.

Because of these two reasons, the POD method will be selected as the reduction technique for the CoPro case studies where partial differential equations are involved.

In case the POD method is not used for parameter estimation purposes, i.e. if model parameters are known, a more efficient model can be developed by just considering snapshots corresponding to simulations performed with the value of the parameters.

3 References

Alonso, A., Frouzakis, C. & Kevrekidis, I., 2004. Optimal sensor placement for state reconstruction of distributed process systems. *AIChE Journal,* 50(7), pp. 1438-1452.

Balsa-Canto, E., Alonso, A. & Banga, J., 2004. Reduced-order models for nonlinear distributed process systems and their application in dynamic optimization. *Industrial & Engineering Chemistry Research,* 43(13), pp. 3353-3363.

Balsa-Canto, E., Banga, J. & Alonso, A., 2002. A novel, efficient and reliable method for thermal process design and optimization. Part II: applications. *Journal of Food Engineering,* 52(3), p. 235.247.

Berkooz, G., Holmes, P. & Lumley, J., 1993. The Proper Orthogonal Decomposition in the analysis of turbulent flows. *Ann. Rev. Fluid Mech.,* Volume 25, pp. 539-575.

Courant, R. & Hilbert, D., 1989. *Methods of Mathematical Physics.* 1st ed. New York: John Wiley & Sons.

Eidelman, Y., Milman, V. D. & Tsolomitis, A., 2004. *Functional analysis : an introduction.* s.l.:American Mathematical Society.

Emirsjlow, Z. & Townley, S., 2000. From PDEs with boundary control to the abstract state equation with an unbounded input operator: a tutorial. *European Journal of Control,* 6(1), pp. 27-49.

Fletcher, C. A. J., 1984. Computational Galerkin Methods. In: Computational Galerkin Methods. Springer Series in Computational Physics. Springer, Berlin, Heidelberg, pp. 72-85.

García, M. R., Vilas, C., Banga, J. R. & Alonso, A. A., 2007. Optimal Field Reconstruction of Distributed Process Systems from Partial Measurements. *Industrial & Engineering Chemistry Research,* 1, 46(2), pp. 530-539.

Holmes, P. y otros, 1997. Low-dimensional models of coherent structures in turbulence. *Physics Reports,* 287(4), pp. 338-384.

Lorenz, E. N., 1960. Energy and Numerical Weather Prediction. *Tellus.*

Reddy, B. D., 1998. *Introductory functional analysis : with applications to boundary value problems and finite elements.* New York: Springer.

Reddy, J., 1993. *An introduction to the finite element method.* Second ed. Boston: McGraw-Hill.

Rudin, W., 1991. *Functional analysis.* s.l.:McGraw-Hill.

Shvartsman, S. Y. & Kevrekidis, I. G., 1998. Nonlinear model reduction for control of distributed systems: A computer-assisted study. *AIChE Journal,* 1 7, 44(7), pp. 1579-1595.

Sirovich, L., 1987. Turbulence and the dynamics of coherent structures. Part I: Coherent structures. *Quaterly of Appl. Math.,* 45(3), pp. 561-571.

Vilas, C., 2008. *Modelling, simulation and robust control of distributed processes: application to chemical and biological systems,* Vigo: http://digital.csic.es/bitstream/10261/4236/1/Carlos%20Vilas.pdf.

Vilas, C. Arias-Méndez, A., García, M. R., Alonso, A. A., & Balsa-Canto, E., 2018. Toward predictive food process models: A protocol for parameter estimation. Critical reviews in food science and nutrition, 58(3), 436-449..

Vilas, C., García, M., Banga, J. & Alonso, A., 2008. Robust feed-back control of travelling waves in a class of reaction–diffusion distributed biological systems. *Physica D - Nonlinear phenomena,* 237(18), pp. 2353-2364.